Published in final edited form as:
Am J Physiol Lung Cell Mol Physiol. 2007 August ; 293(2): L436–L445.

MAPK and heat shock protein 27 activation are associated with respiratory syncytial virus induction of human bronchial epithelial monolayer disruption

Divyendu Singh, **Kelly L. McCann**, and **Farhad Imani**
Laboratory of Respiratory Biology, National Institute of Environmental Health Sciences, National Institutes of Health, Research Triangle Park, North Carolina

Abstract

Singh D, McCann KL, Imani F. MAPK and heat shock protein 27 activation are associated with respiratory syncytial virus induction of human bronchial epithelial monolayer disruption. *Am J Physiol Lung Cell Mol Physiol* 293: L436–L445, 2007. First published June 8, 2007; doi:10.1152/ajplung.00097.2007.—Respiratory syncytial virus (RSV) is the major cause of bronchiolitis in infants, and a common feature of RSV infections is increased lung permeability. The accumulation of fluid in the infected lungs is caused by changes in the endothelial and epithelial membrane integrity. However, the exact mechanisms of viral-induced fluid extravasation remain unclear. Here, we report that infection of human epithelial cells with RSV results in significant epithelial membrane barrier disruption as assessed by a decrease in transepithelial electrical resistance (TEpR). This decrease in TEpR, which indicates changes in paracellular permeability, was mediated by marked cellular cytoskeletal rearrangement. Importantly, the decrease in TEpR was attenuated by using p38 MAPK inhibitors (SB-203580) but was partially affected by JNK inhibitor SP-600125. Interestingly, treatment of A549 cells with MEK1/2 inhibitor (U-0126) led to a decrease in TEpR in the absence of RSV infection. The changes in TEpR were concomitant with an increase in heat shock protein 27 (Hsp27) phosphorylation and with actin microfilament rearrangement. Thus our data suggest that p38 MAPK and Hsp27 are required for RSV induction of human epithelial membrane permeability.

Keywords

lung permeability; mitogen-activated protein kinase

Respiratory Syncytial Virus (RSV), a negative-stranded non-segmented RNA virus, is the most common cause of respiratory tract viral infection in children, and nearly all children are exposed to this virus by age two (18). During respiratory virus infections, including infections with RSV, there is a significant increase in lung permeability, which allows cell and fluid migration into the lung air spaces. The accumulation of fluid in the infected lungs is, in part, caused by changes in the endothelial and epithelial membrane integrity. Fluid extravasation during infections can cause alveolar flooding, rhinorrhea, middle ear effusions, and an increase in respiratory bacterial infections (5,11,33,40,46). Viral-induced fluid extravasation is also a common feature of viral hemorrhagic diseases (35).

RSV infections can lead to severe respiratory infections in the elderly and immunocompromised individuals (44). RSV can also induce other severe respiratory infections such as acute respiratory distress syndrome and acute lung injury, both of which involve

Address for reprint requests and other correspondence: F. Imani, National Institutes of Health/National Institute of Environmental Health Sciences MD 2-01, 111 Alexander Dr., Research Triangle Park, NC 27709 (e-mail: imani@niehs.nih.gov).

endothelial and epithelial membrane dysfunction (8,19,46). RSV infection starts in the upper airway epithelial cells, but it can spread to the lower airways and cause severe bronchiolitis, which is manifested by inflammatory cell infiltration, mucus secretion, and edema (12,18,36, 41). However, the exact mechanisms of viral induced fluid extravasation remain unclear.

Recently, a report by Kilani et al. (27) showed that RSV induction of human epithelial membrane permeability was due to the expression of VEGF. We (8) previously reported that infection of human endothelial cells with bluetongue virus (BTV), a hemorrhagic fever virus of the ruminants, caused transendothelial barrier disruption. The BTV-induced endothelial barrier dysfunction was mediated by the activation of p38 MAPK pathway, which has been established as a critical signaling pathway for vascular endothelial permeability induced by different stimuli (2,3).

The interrelated MAPK pathways are exemplified by the p38 MAPK, ERK, and JNK pathways. These serine/threonine protein kinases are activated by a variety of intracellular and extracellular stimuli including viral infection (10,15,16,20,30,34). After stimulation, p38 MAPK, JNK, and ERK activate several downstream transcription factors such as STAT-1, activating transcription factor-2, and Ets domain-containing protein (Elk-1), which are involved in regulation of inflammation (6,14,22). Moreover, through MAPK-activated protein kinase-2, p38 MAPK activates heat shock protein 27 (Hsp27) by phosphorylation on several different sites such as Ser15, Ser78, Ser82, and Thr143 (7). Hsp27 then regulates cell shape changes by causing dynamic rearrangement of cytoskeletal proteins such as actin (7).

In this study, we have examined the mechanism for disruption of lung epithelial membrane integrity by RSV infection in an in vitro model. Our data, using primary human bronchial epithelial (PHBE) and A549 human alveolar epithelial cells, showed that infection with RSV diminished membrane barrier integrity as assessed by a decrease in transepithelial electrical resistance (TEpR). Our data further showed that using a pharmacological inhibitor of p38 MAPK reduced RSV induction of epithelial membrane permeability. Under identical conditions, inhibition of ERK and JNK led to modest changes in RSV induction of membrane permeability.

The reduction in membrane integrity was not due to virus-induced apoptosis as determined by annexin V and 4,6-dia-midino-2-phenylindole (DAPI) staining. There was, however, a concomitant increase in virus-induced Hsp27 phosphorylation, which was attenuated by treatment of the cells with p38 MAPK inhibitor before infection. Our data provide a molecular mechanism for RSV induction of epithelial barrier disruption and fluid/cell extravasation.

MATERIALS AND METHODS

Cell culture and reagents

PHBE cells were purchased from Cambrex Bio Science (Walkersville, MD) and grown in serum-free bronchial epithelial basal medium-2 with supplements according to the supplier's protocol. Human alveolar basal epithelial cells (A549) were grown at 37°C in 5% CO_2 in DMEM/Ham's F-12 supplemented with 5% heat-inactivated fetal bovine serum (HyClone, Logan, UT), penicillin, and streptomycin.

Pharmacological inhibitors of p38 SB-203580 [4-(4-fluorophenyl)-2-(4-methylsulfinylphenyl)-5-(4-pyridyl)1H-imidazole] or SB-239063 [*trans*-1-(4-hydroxycyclohexyl)-4-(4-fluorophenyl)-5-(2-methoxypyridimidin-4-yl)imidazole], JNK inhibitor SP-600125 [anthra(1,9-cd)pyrazol-6(2H)-one 1,9-pyrazoloanthrone], MEK/ERK1/2 inhibitor PD-98059 (2′-amino-3′-methoxyflavone), and MEK inhibitor U-0126 [1,4-diamino-2,3-dicyano-1,4-bis(2-aminophenylthio) butadiene] were purchased from

Calbiochem (San Diego, CA), dissolved in DMSO, aliquoted, and kept frozen until use. Cytochalasin D was purchased from Sigma-Aldrich (St. Louis, MO).

Viral propagation, infection, and UV inactivation

Human RSV subtype A_2 was propagated in human epithelial cell line (HEp-2) cells as described (17). For virus infections, PHBE and A549 cells were first treated with the pharmacological inhibitors of MAPK for 1 h, and then the medium containing the inhibitor was removed, and cells were infected with RSV at the multiplicity of infection (MOI) indicated in the figure legends. After 1 h of incubation at 37°C, complete medium with the appropriate inhibitor was added, and the cells were incubated further before harvesting. Virus stocks were inactivated by a 10-min exposure to UV (254 nm) in a UV cross-linker (Stratagene, La Jolla, CA).

Transepithelial membrane permeability measurements

Lung epithelial membrane permeability was measured by using an electrical cell-substrate impedance sensing system (ECIS; Applied BioPhysics, Troy, NY) as previously described (4,8). PHBE or A549 cells were plated onto gold-evaporated electrodes (8W10E, Applied BioPhysics) at a density of 150,000 cells per well and grown to a confluent monolayer. Experiments were conducted when the monolayer achieved a resistance of at least 5,000 Ω. As a measure of paracellular contact and permeability, TEpR across the monolayer was measured over time. Based on the analysis of the data using the RbAlpha software (Applied BioPhysics), our data represent alterations in cell-to-cell adhesion and not cell-to-substrate contact. For antibody inhibition assays, neutralizing anti-VEGF was purchased from R&D Systems (Minneapolis, MN). The specific antibody and the isotype control were added to the cell monolayer in the ECIS electrode at 20 μg/ml. The data were normalized to baseline by subtracting the differences in the increased resistance. All of the experiments were performed in duplicate, and the results are presented as means ± SD.

Analysis of cell apoptosis

To assay for RSV-induced apoptosis, A549 cells were infected with RSV for 12 and 24 h and then washed 2× with PBS and stained with FITC-labeled annexin V and propidium iodide (Trevigen, Gaithersburg, MD) according to manufacturer's instructions. Stained cells were subjected to flow cytometry using CellQuest software (BD Biosciences, San Jose, CA). Viability was determined by percentage of double-negative cells compared with total cells (43). Nuclear fragmentation was visualized by using DAPI stain (Molecular Probes, Eugene, OR) followed by confocal microscopy. UV induction of apoptosis in A549 cells was performed as previously described (25). All experiments were performed in duplicate, and the results are presented as means ± SD.

Actin staining, immunostaining, and confocal microscopy

PHBE or A549 cells were grown on sterile coverslips in six-well plates. After virus infection, cells were washed, fixed with 4% formaldehyde, and permeabilized with 0.1% Triton X-100. F-actin was stained with Texas red phalloidin (0.165 μM), and monomeric G-actin was stained with Alexa Fluor 488-labeled DNase I (0.3 μM) for 30 min. Nuclei were then stained with DAPI in ProLong Gold anti-fade solution (Molecular Probes).

For immunostaining using anti-RSV, A549 cells were grown as a confluent monolayer on coverslips. After infection with RSV at indicated MOI, cells were fixed with 4% paraformaldehyde and permeabilized with 0.1% Triton X-100. FITC-conjugated anti-RSV (Chemicon, Temecula, CA) was added to the cells at 1:150 dilution in 1% BSA in PBS-T (PBS with 0.05% Tween 20). After overnight incubation, cells were washed 2× with PBS-T.

Confocal microscopy for the detection of cellular changes were performed using a Zeiss LSM 510 UV META laser scanning confocal microscope (Carl Zeiss MicroImaging, Thornwood, NY) under a ×40 objective lens. All images were analyzed for total fluorescence by using NIH ImageJ software.

Cellular protein extraction and Western blot analysis

Cells were infected with RSV at MOI of 2.5 plaque-forming units (pfu)/cell. After 24 h, medium was removed, and cells were washed 2× with PBS. Equal numbers of cells were lysed using 1× SDS sample buffer containing 2.5% 2-mercaptoethanol. The proteins were denatured and reduced by heating the samples at 95°C for 3 min. The chromosomal DNA was then sheared by passing the samples through a 26-gauge needle several times. The proteins were resolved on a 10 or 12% SDS-PAGE and then electrotransferred onto nitrocellulose membranes.

Proteins were identified by using antibodies to phosphorylated and nonphosphorylated forms of p38 MAPK, JNK, ERK, and Hsp27 (Cell Signaling Technology, Beverly, MA) and used according to the manufacturer's protocol. The immunoblotted proteins were then visualized by using the ECL Western blot detection system (GE Healthcare Bio-Sciences, Piscataway, NJ).

RESULTS

RSV infection induces epithelial monolayer disruption as measured by changes in TEpR

The epithelial monolayer plays a critical role in lung permeability (21). To test whether RSV infection induced changes in epithelial monolayer integrity, we have used a method to detect changes in membrane electrical resistance in real-time. Confluent monolayers of PHBE or A549 cells were infected with RSV at different MOI (Fig. 1, *A* and *B*), and TEpR was continuously measured using an ECIS instrument. The data in Fig. 1, *A* and *B*, show that RSV infection induced a concentration-dependent decrease in epithelial monolayer resistance. The decrease in resistance was first detected at 5–10 h postinfection for the two different cell types, and the resistance continued to decrease 25–30% over time. As a control, we used UV-inactivated RSV in A549 cells, which did not induce any decrease in TEpR when added at MOI of 5 pfu/cell, suggesting that virus replication is required for the observed effects.

Decrease in TEpR is not due to apoptosis but due to paracellular contact

The decrease in RSV-induced TEpR suggests an enhancement of paracellular permeability or viral-induced cell death perhaps by apoptosis. To test these possibilities, we first examined RSV induction of apoptosis in A549 cells. Cells were infected with RSV at MOI of 2.5 pfu/cell, and the apoptosis was then measured first by annexin V staining. Data in Fig. 2*A* showed that there was no significant increase in apoptosis at 12- or 24-h time points. As a positive control, A549 cells were treated with UV for 30 min and then incubated overnight to induce apoptosis (Fig. 2 *A*). In addition to annexin V staining, we also examined the late apoptotic events by visualizing the presence of nuclear fragmentation by DAPI staining of infected cells. The data in Fig. 2*B* showed that RSV infection at MOI of 5 pfu/cell after 24 h did not induce nuclear fragmentation in A549 cells. In contrast to RSV infection, UV treatment of A549 cells for 30 min induced marked nuclear fragmentation (Fig. 2*B*).

Since the data in Fig. 2, *A* and *B*, showed that there was no increase in apoptosis, we next examined whether there was paracellular gap formation. Confluent monolayers of A549 cells were either mock infected or infected at an increasing MOI as indicated in Fig. 2*C*. After 24 h, cells were stained with Texas red phalloidin to visualize actin microfilaments. The data in Fig. 2*C* showed that RSV infection resulted in a dose-dependent gap formation. This suggested

that, in agreement with data reported by Kiani et al. (26), RSV-induced decrease in TEpR was due primarily to paracellular gap formation.

RSV activation of MAPK pathway is necessary for changes in TEpR

Since data from our group and others have shown that MAPK pathway is involved in endothelial permeability (3,8), we next examined the role of p38, JNK, and ERK in RSV induction of epithelial membrane disruption. First, we determined the effect of pharmacological inhibitors on their targets during RSV infection of A549 cells. Cells were treated with p38 MAPK inhibitor (SB-203580; Fig. 3*A*), inhibitor of JNK (SP-600125; Fig. 3*B*), or inhibitor of ERK (U-0126; Fig. 3*C*) for 1 h before infection with RSV at MOI of 2.5 pfu/cell. Cells were harvested after 24 h of infection, and total cellular proteins were extracted and used in Western blot analysis. The data in Fig. 3 showed that RSV activated MAPK pathways, and the inhibitors effectively attenuated the virus-induced MAPK activation.

We next examined the effect of the MAPK inhibitors on viral-induced changes in TEpR. Confluent monolayers of A549 and PHBE cells were treated with each MAPK inhibitor at optimal concentration for 1 h before infection with RSV at MOI of 2.5 pfu/cell. The change in TEpR was then continuously measured. Data in Fig. 4*A* showed that inhibition of p38 MAPK significantly attenuated RSV induction of membrane disruption in both A549 and PHBE cells. Inhibition of JNK partially attenuates reduction in TEpR in A549 and in PHBE cells (Fig. 4*B*). However, inhibition of ERK pathway resulted in attenuation of TEpR changes only during early times after RSV infection (Fig. 4*C*). However, at later times postinfection, inhibition of ERK had no effect on RSV-induced TEpR changes. It is important to mention that treatment of A549 but not PHBE cells with the ERK inhibitor (U-0126) pathway resulted in a significant decrease in TEpR without viral infection, suggesting that there are differences between primary epithelial and A549 cells in the regulation of cellular gap junctions.

RSV infection induces cytoskeletal rearrangement in epithelial cells

A critical step for cell shape changes allowing for paracellular gap formation is actin microfilament rearrangement (39). To determine the effect of RSV infection on actin microfilament rearrangement, we infected A549 cells with RSV at MOI of 2.5 pfu/cell. After 24 h, actin was visualized by staining with Texas red phalloidin (Fig. 5*A*) for filamentous form and with Alexa Fluor 488-labeled DNase I staining for the globular form. In contrast to mock infected cells, which showed a relatively equal distribution of filamentous and globular actin, RSV infection resulted in potent cytoskeletal rearrangement as detected by an increase in filamentous actin polymerization.

We next examined the effect of MAPK inhibitors on RSV induction of cytoskeletal rearrangement from globular to filamentous (Fig. 5*A*). Cells were treated with the MAPK inhibitors for 1 h and then infected with RSV at MOI of 2.5 pfu/cell. After 24 h, cells were stained with Texas red phalloidin for the filamentous form and Alexa Fluor 488-labeled DNase I for the globular form of actin. We then quantified actin polymerization in data obtained in Fig. 5*A* by determining the ratio of filamentous-to-globular actin (Fig. 5*B*). The data in Fig. 5 showed that the p38 MAPK inhibitor significantly attenuated RSV induction of actin polymerization.

RSV infection activates Hsp27

It has been established that polymerization of actin and corresponding cell shape changes are mediated through the activation of Hsp27 by p38 MAPK (31). To address the involvement of Hsp27 in RSV induction of epithelial monolayer disruption, we first performed Western blot analysis detecting the phosphorylation state of Hsp27 on two critical residues, Ser78 and Ser82 (Fig. 6). A549 cells were treated with different MAPK inhibitors for 1 h before infection with

RSV at MOI of 2.5 pfu/cell. After 24 h, total cellular proteins were separated by electrophoresis, and phosphorylation state of Hsp27 was determined by Western blot analysis using specific antibodies to phosphorylated forms of Hsp27 on Ser78 and Ser82.

Data in Fig. 6*A* showed that RSV infection induced phosphorylation of Hsp27 on both residues, Ser82 and Ser78. The increase in Hsp27 phosphorylation was potently attenuated by treatment of the cells with p38 MAPK inhibitor SB-203580 (Fig. 6*B*). Addition of the JNK inhibitor SP-600125 did not have an appreciable effect on Hsp27 phosphorylation. In contrast, the ERK inhibitor U-0126 enhanced RSV induction of Hsp27 phosphorylation (Fig. 6*C*), which is consistent with the data obtained from TEpR experiments when using A549 cells (Fig. 4*C*, *top*).

DISCUSSION

An important complication of respiratory viral infections such as infection with RSV is fluid extravasation into the lung air spaces. This requires, in part, dysregulation of epithelial membrane barrier function. The increase of fluid in the lung air spaces can lead to pneumonia and secondary bacterial infections (21). Thus far, the molecular mechanisms for viral-induced epithelial membrane permeability have not been fully elucidated. In this report, we show for the first time that infection of human epithelial cells with RSV leads to activation of MAPK pathways, Hsp27 phosphorylation, actin microfilament rearrangement, cell shape changes, and gap formation, which subsequently leads to epithelial permeability.

Infection of PHBE and A549 cells with RSV led to a dose-dependent decrease in TEpR as measured by ECIS. This decrease in TEpR was a function of live virus and was not affected by UV-inactivated RSV particles. Since ECIS measurements are a function of cell-to-cell contact, our data suggest that there was virus-induced paracellular membrane permeability. Since VEGF has been reported to induce endothelial and epithelial monolayer disruption (1, 27), we have examined whether the RSV-induced reduction in monolayer integrity was due to secretion of VEGF. Confluent A549 monolayers either were infected with RSV at MOI of 5 pfu/cell or were first treated with neutralizing anti-VEGF antibody at 20 μg/ml and then infected. Data from the ECIS experiments showed that the presence of anti-VEGF had a partial (~28% decrease) and reproducible effect on the early events, between 8–16 h postinfection, which continued overtime (data not shown). This is similar but not identical to data obtained by Kilani et al. (27). The difference may likely be due to the dose of virus used in experiments by Kilani et al. (Ref. 27; 0.05 and 0.5 pfu/cell) and in our experiments (2.5 and 5 pfu/cell).

Kotelkin et al. (28) reported that RSV infection can induce apoptosis; therefore, we performed annexin V staining of the cells after RSV infection. Our flow cytometry data showed that RSV infection did not induce apoptosis in A549 cells at 24 h postinfection. In addition, nuclear staining with DAPI did not show any morphological changes in the nuclei such as fragmentation, which is a hallmark of cells undergoing apoptosis (23). As expected, UV treatment of A549 cells induced marked nuclear fragmentation (Fig. 2*A*).

Paracellular gap formation is the result of changes in adherens and tight junctions. Intracellular regulation of tight junctions is mediated by cytoskeletal actin microfilament organization, and actin rearrangement is associated with membrane barrier function. Actin is present as polymeric filamentous (F) and monomeric globular (G) forms, and the reorganization of actin between these two forms regulates cell shape changes (38). To assess the role of actin in RSV induction of membrane permeability, we performed fluorescent staining of filamentous actin with Texas red phalloidin and globular actin with Alexa Fluor 488-labeled DNase I. Our data showed that RSV infection resulted in potent reorganization of actin from G to F form, which leads to cellular contraction and gap formation (Fig. 5, *B* and *C*). This is in agreement with our

hypothesis that RSV induction of epithelial permeability is through reduction of cellular contact.

Recent reports by Birukova et al. (2) showed that actin reorganization and paracellular gap formation in endothelial membrane were mediated by activation of MAPK pathway, which led to downstream activation of Hsp27. We (8) have recently reported that infection of endothelial cells with BTV, a hemorrhagic virus, resulted in the induction of membrane permeability through the activation of p38 MAPK pathway.

In this report, we have used pharmacological inhibitors of p38 MAPK, JNK, and ERK to address the role of MAPK pathways in RSV induction of membrane permeability. Our data showed that inhibition of p38 MAPK resulted in a significant attenuation of RSV-induced gap formation as assessed by ECIS and fluorescent staining. This is consistent with previous data from our lab (8) and others (3) that showed that p38 MAPK was critically involved in endothelial membrane permeability. Our data further showed that JNK inhibition partially affected RSV induction of epithelial permeability. Inhibition of ERK signaling in A549 cells led to a reduction in TEpR in the absence of RSV infection, suggesting a role for ERK in basal regulation of membrane integrity at least in this cell line. In contrast, treatment of PHBE cells with ERK inhibitor alone did not have any significant effect on basal or viral-induced permeability (Fig. 4*C*), suggesting that in primary epithelial cells, ERK does not have a role in membrane integrity. At this point, the difference between A549 and primary epithelial cells in the role of ERK in basal regulation of cellular contact is not clear, but it could be due to the lack of tight junctions in A549 cells (13,42). Both adherens and tight junctions are present in primary epithelial cells.

It is well-established that subsequent to p38 MAPK activation, Hsp27 phosphorylation mediates actin reorganization leading to cell shape changes (32). The phosphorylation of Hsp27 is protective against stress-induced actin fragmentation, whereas in nonphosphorylated form, it can prevent actin polymerization (24,38). It has been reported that Hsp27 phosphorylation on several residues including Ser78 and Ser82 necessary for actin rearrangement (7,31). We, therefore, examined the effect of RSV infection on Hsp27 activation Western blot analysis. Our data showed that RSV infection resulted in phosphorylation of Hsp27 on both Ser78 and Ser82.

In agreement with data obtained from experiments of TEpR using ECIS instrument, treatment of the cells with the p38 MAPK inhibitor attenuated RSV-induced phosphorylation of Hsp27 (Fig. 6). Interestingly, inhibition of ERK signaling enhanced Hsp27 phosphorylation. This is consistent with our data showing that in the absence of RSV infection, ERK inhibition increased membrane permeability in A549 cells (Fig. 4*C*). Addition of ERK inhibitor alone to the cells resulted in an increase in basal activation of Hsp27 (data not shown). The reason for this observation is not yet clear, but it may suggest a complex interplay between MAPK pathways in maintaining basal membrane barrier function in some cell types.

Recently, Kunzelmann et al. (29) reported that RSV infection induced fluid accumulation in the lungs by inhibition of airway sodium transport. It also has been reported that secretion of cytokines such as TNF-α and VEGF contributes to endothelial and epithelial permeability (9, 27,37,45). At this point, the exact mechanism of virus-induced permeability is not clear. Our data revealed that RSV infection resulted in activation of p38 MAPK and Hsp27 phosphorylation. These signal transduction events led to actin microfilament rearrangement, cell shape changes, and paracellular gap formation. We believe that disruption of membrane barrier function by paracellular gap formation is a likely mechanism for fluid and cell extravasation into the lung air spaces.

At this point, it is not clear whether RSV-induced formation is a direct intracellular effect or occurs through secretion of cytokines. Based on our observations and data provided by Kilani et al. (27), we speculate that both mechanisms may be involved. Our future experiments will be aimed at delineating the exact virally activated signal transduction pathways that participate in RSV-induced gap formation.

Acknowledgements

GRANTS This research was supported by the Intramural Research Program of the National Institutes of Health, National Institute of Environmental Health Sciences.

REFERENCES

1. Becker PM, Verin AD, Booth MA, Liu F, Birukova A, Garcia JG. Differential regulation of diverse physiological responses to VEGF in pulmonary endothelial cells. Am J Physiol Lung Cell Mol Physiol 2001;281:L1500–L1511. [PubMed: 11704547]
2. Birukova AA, Birukov KG, Gorshkov B, Liu F, Garcia JG, Verin AD. MAP kinases in lung endothelial permeability induced by microtubule disassembly. Am J Physiol Lung Cell Mol Physiol 2005;289:L75–L84. [PubMed: 15778245]
3. Borbiev T, Birukova A, Liu F, Nurmukhambetova S, Gerthoffer WT, Garcia JG, Verin AD. p38 MAP kinase-dependent regulation of endothelial cell permeability. Am J Physiol Lung Cell Mol Physiol 2004;287:L911–L918. [PubMed: 15475493]
4. Borbiev T, Verin AD, Shi S, Liu F, Garcia JG. Regulation of endothelial cell barrier function by calcium/calmodulin-dependent protein kinase II. Am J Physiol Lung Cell Mol Physiol 2001;280:L983–L990. [PubMed: 11290523]
5. Bousquet J, Jeffery PK, Busse WW, Johnson M, Vignola Asthma AM. From bronchoconstriction to airways inflammation and remodeling. Am J Respir Crit Care Med 2000;161:1720–1745. [PubMed: 10806180]
6. Brinkman BM, Telliez JB, Schievella AR, Lin LL, Goldfeld AE. Engagement of tumor necrosis factor (TNF) receptor 1 leads to ATF-2-and p38 mitogen-activated protein kinase-dependent TNF-alpha gene expression. J Biol Chem 1999;274:30882–30886. [PubMed: 10521481]
7. Butt E, Immler D, Meyer HE, Kotlyarov A, Laass K, Gaestel M. Heat shock protein 27 is a substrate of cGMP-dependent protein kinase in intact human platelets: phosphorylation-induced actin polymerization caused by HSP27 mutants. J Biol Chem 2001;276:7108–7113. [PubMed: 11383510]
8. Chiang ET, Persaud-Sawin DA, Kulkarni S, Garcia JG, Imani F. Bluetongue virus and double-stranded RNA increase human vascular permeability: role of p38 MAPK. J Clin Immunol 2006;26:406–416. [PubMed: 16786433]
9. Clements RT, Minnear FL, Singer HA, Keller RS, Vincent PA. RhoA and Rho-kinase dependent and independent signals mediate TGF-β-induced pulmonary endothelial cytoskeletal reorganization and permeability. Am J Physiol Lung Cell Mol Physiol 2005;288:L294–L306. [PubMed: 15475381]
10. Cobb MH. MAP kinase pathways. Prog Biophys Mol Biol 1999;71:479–500. [PubMed: 10354710]
11. Cretney E, Shanker A, Yagita H, Smyth MJ, Sayers TJ. TNF-related apoptosis-inducing ligand as a therapeutic agent in autoimmunity and cancer. Immunol Cell Biol 2006;84:87–98. [PubMed: 16405656]
12. Doyle WJ, Gentile DA, Skoner DP. Viral and bacterial rhinitis. Clin Allergy Immunol 2007;19:177–195. [PubMed: 17153013]
13. Duff C, Murphy PG, Callaghan M, McClean S. Differences in invasion and translocation of *Burkholderia cepacia* complex species in polarised lung epithelial cells in vitro. Microb Pathog 2006;41:183–192. [PubMed: 16938423]
14. Enslen H, Tokumitsu H, Stork PJ, Davis RJ, Soderling TR. Regulation of mitogen-activated protein kinases by a calcium/calmodulin-dependent protein kinase cascade. Proc Natl Acad Sci USA 93;1996:10803–10808.
15. Fearns C, Kline L, Gram H, Di Padova F, Zurini M, Han J, Ulevitch RJ. Coordinate activation of endogenous p38alpha, beta, gamma, and delta by inflammatory stimuli. J Leukoc Biol 2000;67:705–711. [PubMed: 10811012]

16. Garrington TP, Johnson GL. Organization and regulation of mitogen-activated protein kinase signaling pathways. Curr Opin Cell Biol 1999;11:211–218. [PubMed: 10209154]
17. Graham BS, Perkins MD, Wright PF, Karzon DT. Primary respiratory syncytial virus infection in mice. J Med Virol 1988;26:153–162. [PubMed: 3183639]
18. Hall CB. Respiratory syncytial virus and parainfluenza virus. N Engl J Med 2001;344:1917–1928. [PubMed: 11419430]
19. Hammer J, Numa A, Newth CJ. Acute respiratory distress syndrome caused by respiratory syncytial virus. Pediatr Pulmonol 1997;23:176–183. [PubMed: 9094725]
20. Hedges JC, Singer CA, Gerthoffer WT. Mitogen-activated protein kinases regulate cytokine gene expression in human airway myocytes. Am J Respir Cell Mol Biol 2000;23:86–94. [PubMed: 10873157]
21. Hippenstiel S, Opitz B, Schmeck B, Suttorp N. Lung epithelium as a sentinel and effector system in pneumonia–molecular mechanisms of pathogen recognition and signal transduction. Respir Res 2006;7:97. [PubMed: 16827942]
22. Hodge C, Liao J, Stofega M, Guan K, Carter-Su C, Schwartz J, Enslen H, Tokumitsu H, Stork PJ, Davis RJ, Soderling TR. Growth hormone stimulates phosphorylation and activation of Elk-1 and expression of c-*fos*, *egr*-1, and *junB* through activation of extracellular signal-regulated kinases 1 and 2. Regulation of mitogen-activated protein kinases by a calcium/calmodulin-dependent protein kinase cascade. J Biol Chem 1998;273:31327–31336. [PubMed: 9813041]
23. Hotz MA, Gong J, Traganos F, Darzynkiewicz Z. Flow cytometric detection of apoptosis: comparison of the assays of in situ DNA degradation and chromatin changes. Cytometry 1994;15:237–244. [PubMed: 8187583]
24. Huot J, Houle F, Spitz DR, Landry J. HSP27 phosphorylation-mediated resistance against actin fragmentation and cell death induced by oxidative stress. Cancer Res 1996;56:273–279. [PubMed: 8542580]
25. Jiang Y, Rom WN, Yie TA, Chi CX, Tchou-Wong KM. Induction of tumor suppression and glandular differentiation of A549 lung carcinoma cells by dominant-negative IGF-I receptor. Oncogene 1999;18:6071–6077. [PubMed: 10557096]
26. Kiani A, Garcia-Cozar FJ, Habermann I, Laforsch S, Aebischer T, Ehninger G, Rao A. Regulation of interferon-gamma gene expression by nuclear factor of activated T cells. Blood 2001;98:1480–1488. [PubMed: 11520798]
27. Kilani MM, Mohammed KA, Nasreen N, Hardwick JA, Kaplan MH, Tepper RS, Antony VB. Respiratory syncytial virus causes increased bronchial epithelial permeability. Chest 2004;126:186–191. [PubMed: 15249461]
28. Kotelkin A, Prikhod'ko EA, Cohen JI, Collins PL, Bukreyev A. Respiratory syncytial virus infection sensitizes cells to apoptosis mediated by tumor necrosis factor-related apoptosis-inducing ligand. J Virol 2003;77:9156–9172. [PubMed: 12915532]
29. Kunzelmann K, Sun J, Meanger J, King NJ, Cook DI. Inhibition of airway Na^+ transport by respiratory syncytial virus. J Virol 2007;81:3714–3720. [PubMed: 17287265]
30. Kyriakis JM, Avruch J. Mammalian mitogen-activated protein kinase signal transduction pathways activated by stress and inflammation. Physiol Rev 2001;81:807–869. [PubMed: 11274345]
31. Landry J, Huot J. Modulation of actin dynamics during stress and physiological stimulation by a signaling pathway involving p38 MAP kinase and heat-shock protein 27. Biochem Cell Biol 1995;73:703–707. [PubMed: 8714691]
32. Landry J, Lambert H, Zhou M, Lavoie JN, Hickey E, Weber LA, Anderson CW. Human HSP27 is phosphorylated at serines 78 and 82 by heat shock and mitogen-activated kinases that recognize the same amino acid motif as S6 kinase II. J Biol Chem 1992;267:794–803. [PubMed: 1730670]
33. Lee CG, Yoon HJ, Zhu Z, Link H, Wang Z, Gwaltney JM, Landry M, Elias JA. Respiratory syncytial virus stimulation of vascular endothelial cell growth factor/vascular permeability factor. Am J Respir Cell Mol Biol 2000;23:662–669. [PubMed: 11062145]
34. Lee JC, Laydon JT, McDonnell PC, Gallagher TF, Kumar S, Green D, McNulty D, Blumenthal MJ, Heys JR, Landvatter SW, Strickler JE, McLaughlin MM, Siemens IR, Fisher SM, Livi GP, White JR, Adams JL, Young PR. A protein kinase involved in the regulation of inflammatory cytokine biosynthesis. Nature 1994;372:739–746. [PubMed: 7997261]

35. Marty AM, Jahrling PB, Geisbert TW. Viral hemorrhagic fevers. Clin Lab Med 2006;26:345–386. [PubMed: 16815457]viii
36. Peebles RS Jr, Graham BS. Pathogenesis of respiratory syncytial virus infection in the murine model. Proc Am Thorac Soc 2005;2:110–115. [PubMed: 16113477]
37. Petrache I, Birukov K, Zaiman AL, Crow MT, Deng H, Wadgaonkar R, Romer LH, Garcia JG. Caspase-dependent cleavage of myosin light chain kinase (MLCK) is involved in TNF-alpha-mediated bovine pulmonary endothelial cell apoptosis. FASEB J 2003;17:407–416. [PubMed: 12631580]
38. Pichon S, Bryckaert M, Berrou E. Control of actin dynamics by p38 MAP kinase - Hsp27 distribution in the lamellipodium of smooth muscle cells. J Cell Sci 2004;117:2569–2577. [PubMed: 15128872]
39. Schnittler HJ, Wilke A, Gress T, Suttorp N, Drenckhahn D. Role of actin and myosin in the control of paracellular permeability in pig, rat and human vascular endothelium. J Physiol 1990;431:379–401. [PubMed: 2100310]
40. Shay DK, Holman RC, Roosevelt GE, Clarke MJ, Anderson LJ. Bronchiolitis-associated mortality and estimates of respiratory syncytial virus-associated deaths among US children 1979–1997. J Infect Dis 2001;183:16–22. [PubMed: 11076709]
41. Tripp RA, Oshansky C, Alvarez R. Cytokines and respiratory syncytial virus infection. Proc Am Thorac Soc 2005;2:147–149. [PubMed: 16113483]
42. Vasioukhin V, Bauer C, Yin M, Fuchs E. Directed actin polymerization is the driving force for epithelial cell-cell adhesion. Cell 2000;100:209–219. [PubMed: 10660044]
43. Vermes I, Haanen C, Steffens-Nakken H, Reutelingsperger C. A novel assay for apoptosis. Flow cytometric detection of phosphatidylserine expression on early apoptotic cells using fluorescein labelled annexin V. J Immunol Methods 1995;184:39–51. [PubMed: 7622868]
44. Whimbey E, Ghosh S. Respiratory syncytial virus infections in immunocompromised adults. Curr Clin Top Infect Dis 2000;20:232–255. [PubMed: 10943527]
45. Willis BC, Kim KJ, Li X, Liebler J, Crandall ED, Borok Z. Modulation of ion conductance and active transport by TGF-β1 in alveolar epithelial cell monolayers. Am J Physiol Lung Cell Mol Physiol 2003;285:L1192–L1200. [PubMed: 12730080]
46. Zaroukian MH, Kashyap GH, Wentworth BB. Respiratory syncytial virus infection: a cause of respiratory distress syndrome and pneumonia in adults. Am J Med Sci 1988;295:218–222. [PubMed: 3354594]

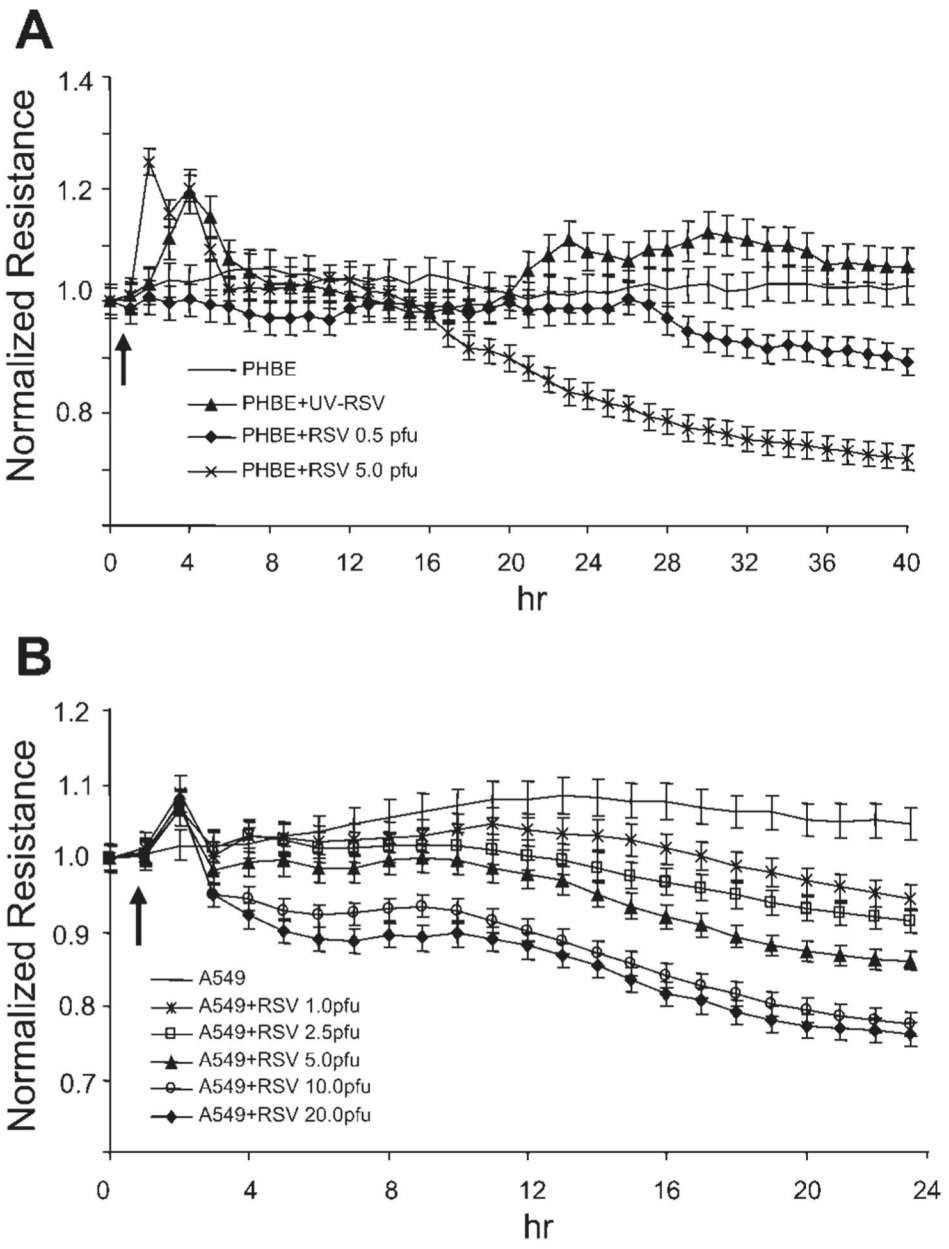

Fig. 1.

Respiratory syncytial virus (RSV) infection reduces transepithelial electrical resistance (TEpR) in human epithelial membranes. Primary human bronchial epithelial (PHBE) cells (*A*) or A549 cells (*B*) were grown as a confluent monolayer on 8-well tissue culture dishes containing gold-plated electrode arrays. The cells were then infected with increasing concentration RSV as indicated in the figure. The TEpR across the membrane was then continuously measured using an electrical cell-substrate impedance sensing (ECIS) instrument. The arrow indicates the start time of virus infection. All experiments were performed in duplicate ($n = 2$). pfu, Plaque-forming units.

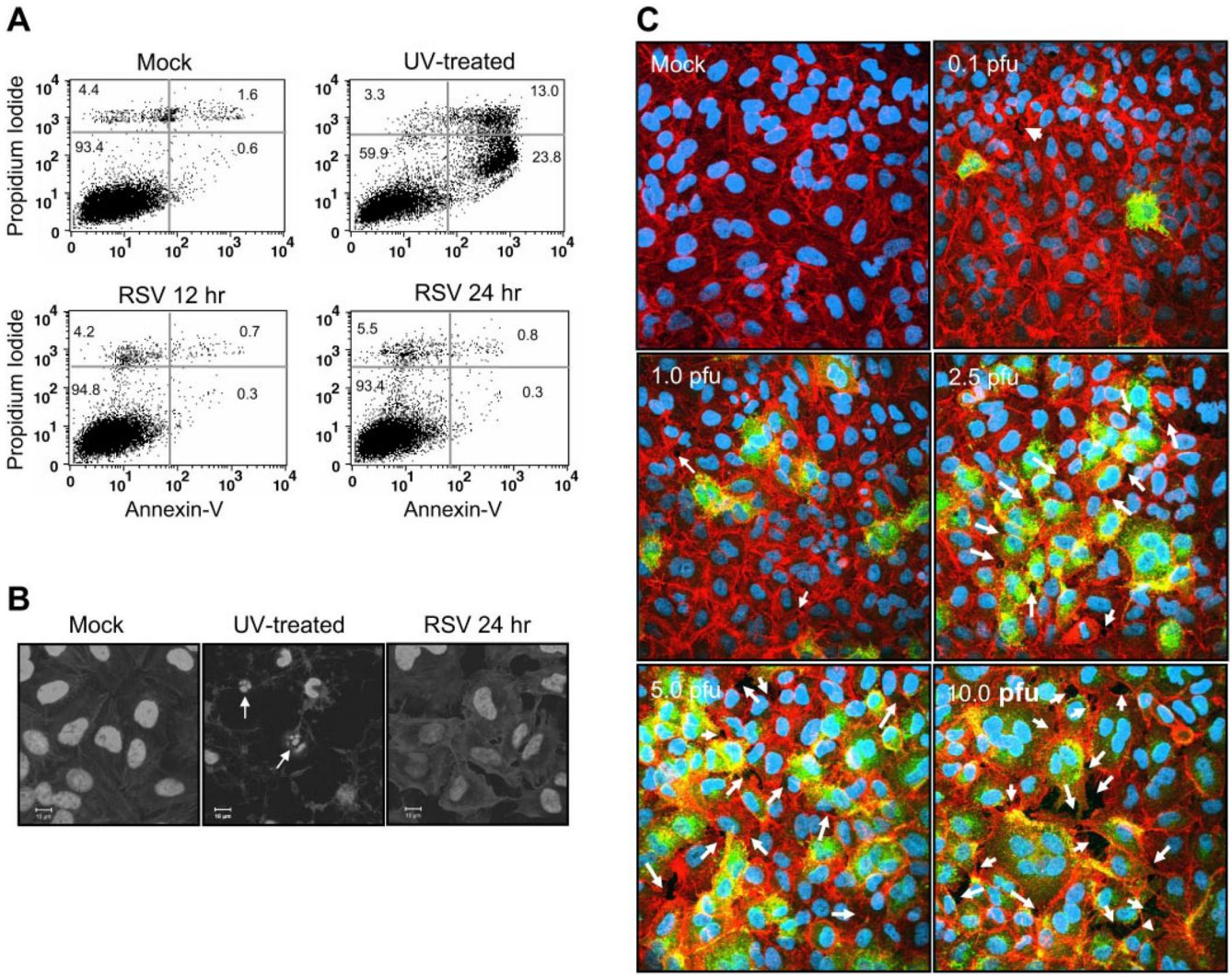

Fig. 2.

RSV infection does not cause apoptosis but causes paracellular gaps. A549 cells were treated with vehicle alone (Mock), treated with UV (30 min) to induce apoptosis, or infected with RSV at multiplicity of infection (MOI) of 2.5 pfu/cell. Apoptosis levels were then determined after further incubation by annexin V staining and flow cytometry (*A*) or with 4,6-diamidino-2-phenylindole (DAPI) nuclear staining (*B*) and confocal microscopy ($n = 3$). Scale bar represents 10 μm. *C*: to test for the presence of paracellular gaps, confluent monolayers of A549 cells were infected with RSV at concentrations indicated in the figure. The cells were then stained with Texas red-phalloidin for actin and DAPI for nuclear staining. RSV-infected cells were visualized by using FITC-labeled goat anti-RSV antibody. Arrows indicate paracellular gaps ($n = 2$).

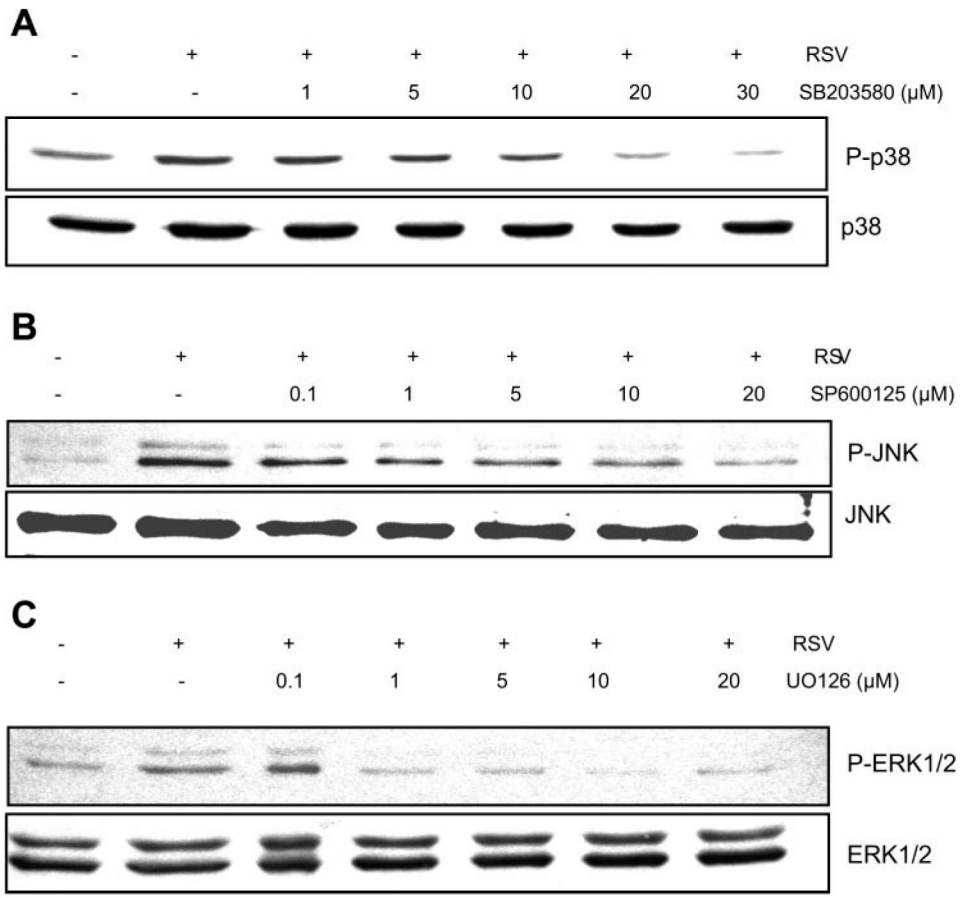

Fig. 3.

Pharmacological inhibitors block RSV activation of MAPK pathways. A549 cells were mock treated (vehicle) or treated with p38 inhibitor (SB-203580; *A*), JNK inhibitor (SP-600125; *B*), or ERK inhibitor (U-0126; *C*) before infection with RSV at MOI of 2.5 pfu/cell. Cellular proteins were separated on 10% SDS-PAGE and blotted using antibodies to the phosphorylated (P) form of the MAPKs followed by visualization using the ECL method. As a control, the blots were stripped and reprobed with specific antibodies to the nonphosphorylated MAPKs ($n = 2$).

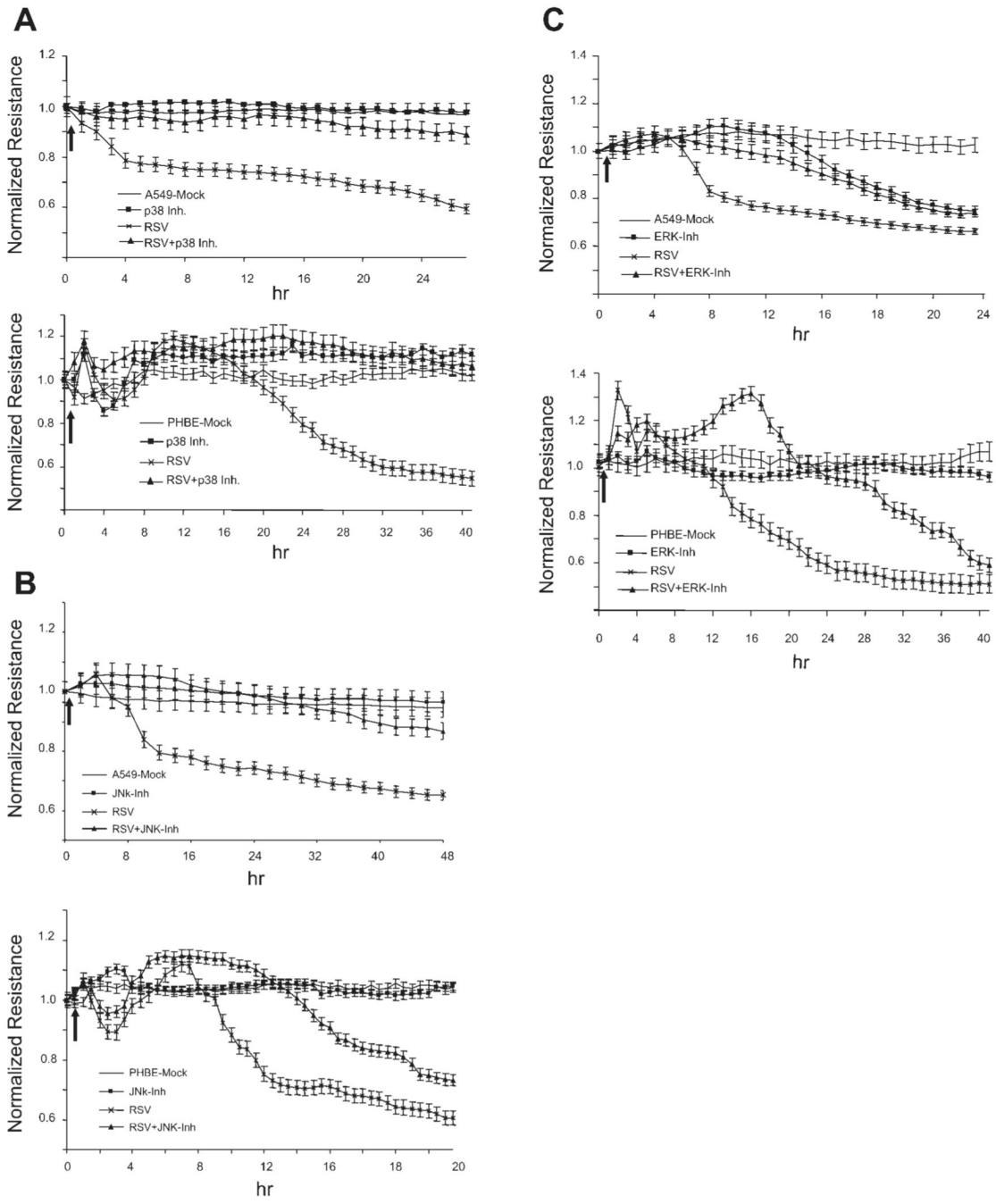

Fig. 4.

Effect of MAPK inhibitors on RSV induction of epithelial membrane disruption. A549 or PHBE cells were mock treated (vehicle) or treated with p38 MAPK inhibitor (*A*) at 20 μM, JNK inhibitor (*B*) at 10 μM, or ERK inhibitor (*C*) at 10 μM for 1 h before infection with RSV at MOI of 2.5 pfu/cell. The electrical resistance was then continuously measured ($n = 4$). The arrow indicates the start of virus infection. Inh, inhibitor.

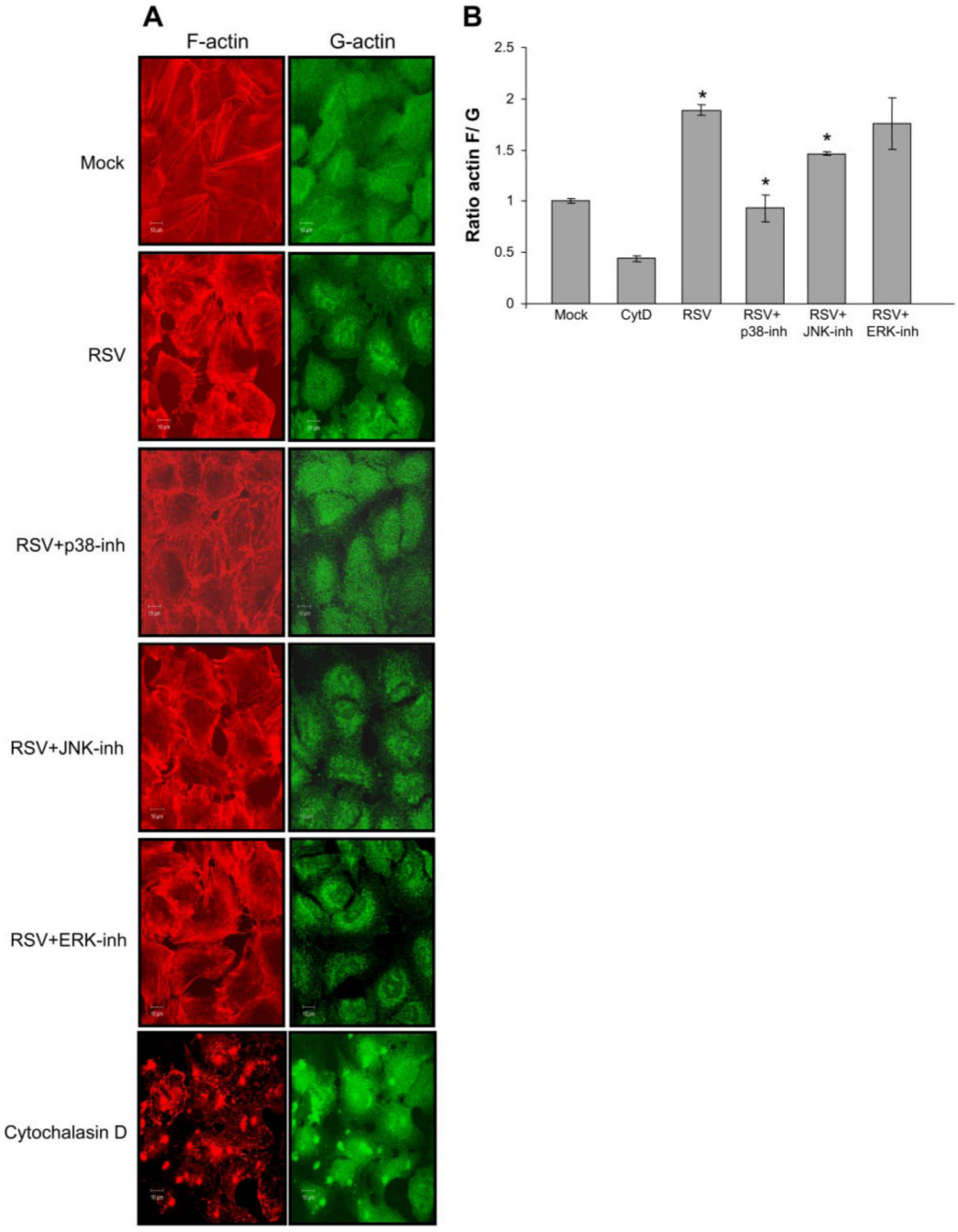

Fig. 5.

RSV infection leads to actin microfilament rearrangement. *A*: A549 cells were infected with RSV at MOI of 2.5 pfu/cell, and after 24 h, filamentous actin was stained with Texas red phalloidin, and G-actin was stained with Alexa Fluor 488-labeled DNase I. Visualization of actin was performed by confocal microscopy. The effect of MAPK inhibition was also determined on RSV-induced changes in actin polymerization; cytochalasin D (control) was used at 5 μM for 4 h ($n = 2$). *B*: the ratio of total filamentous actin-to-globular actin was quantified by comparing stain intensity of Texas red phalloidin to Alexa Fluor 488-labeled DNase I staining obtained in *A*. The error bars indicate the SD of the mean ($n = 2$); $^*P < 0.01$. CytD, cytochalasin D.

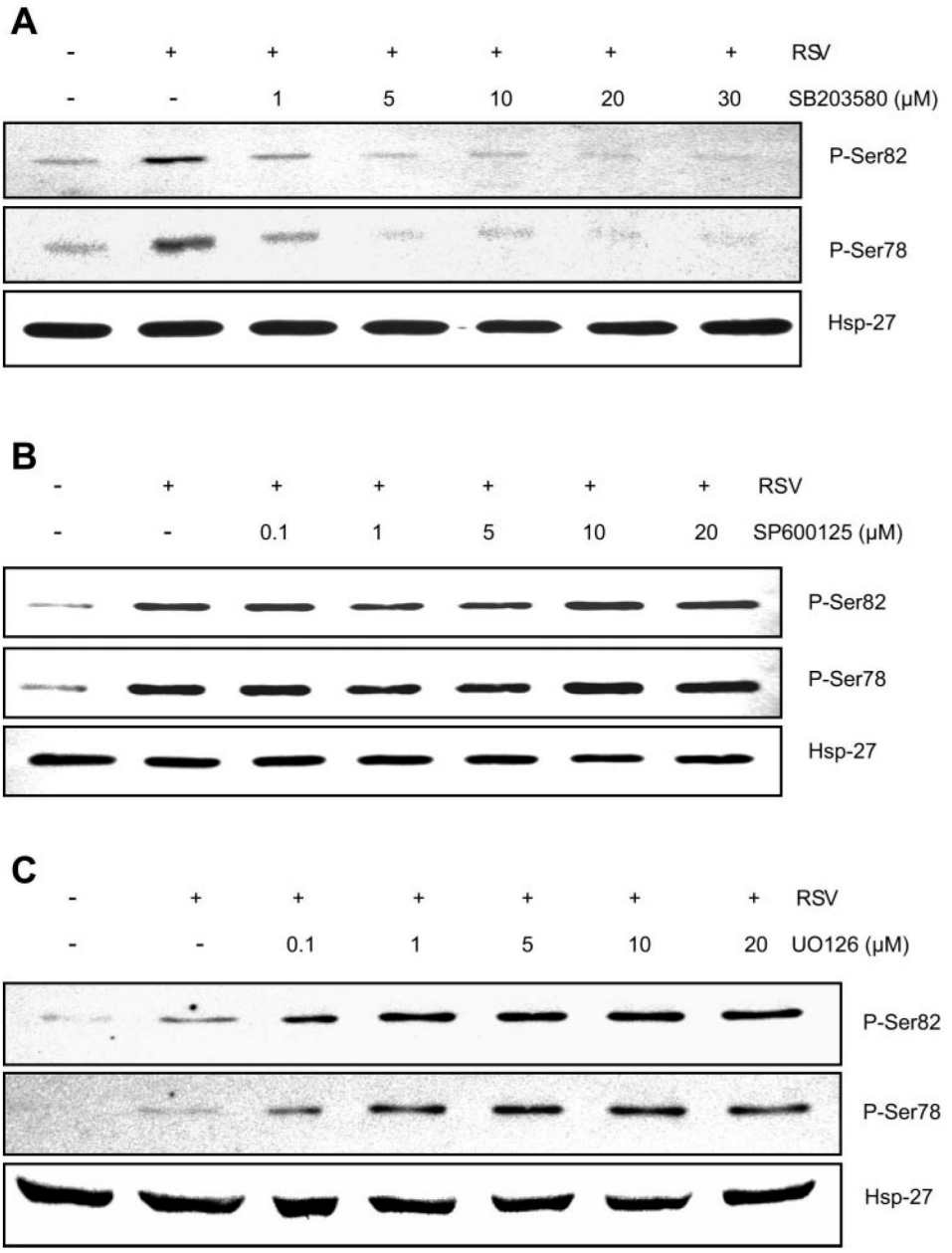

Fig. 6.

A–C: effects of MAPK inhibition on heat shock protein 27 (Hsp27) phosphorylation. A549 cells were mock treated (vehicle), treated with the indicated p38 MAPK inhibitor (*A*), JNK inhibitor (*B*), or ERK inhibitor (*C*) for 1 h before infection with RSV at MOI of 2.5 pfu/cell. After 24 h, total cellular proteins were separated on a 12% SDS-PAGE, and phosphorylation of Hsp27 was determined by Western blot analysis using antibodies specific to phospho-Ser78 and phospho-Ser82. As an internal control, the level of nonphosphorylated Hsp27 was determined by probing identical blots with a specific antibody ($n = 2$).